6652 *Inorg. Chem.* **2009**, *48*, 6652–6660
DOI: 10.1021/ic900621c

Inorganic Chemistry
Article

Porous Manganese(II) 3-(2-Pyridyl)-5-(4-Pyridyl)-1,2,4-Triazolate Frameworks: Rational Self-Assembly, Supramolecular Isomerism, Solid-State Transformation, and Sorption Properties

Jian-Bin Lin, Jie-Peng Zhang,* Wei-Xiong Zhang, Wei Xue, Dong-Xu Xue, and Xiao-Ming Chen*

MOE Key Laboratory of Bioinorganic and Synthetic Chemistry/State Key Laboratory of Optoelectronic Materials and Technologies, School of Chemistry & Chemical Engineering, Sun Yat-Sen University, Guangzhou 510275, China

Received March 31, 2009

Reactions of 3-(2-pyridyl)-5-(4-pyridyl)-1,2,4-triazole (Hdpt24) with $Mn(OAc)_2$ under different conditions give two mononuclear complexes, $[Mn(dpt24)_2(MeOH)_2]$ (**1**) and $[Mn(dpt24)_2(H_2O)_2]\cdot 6H_2O$ (**2**), and three isomeric two-dimensional (2D) coordination polymers α-$[Mn(dpt24)_2]$ (**3a**), β-$[Mn(dpt24)_2]\cdot g$ (**3b**$\cdot$g, g = DMF and H_2O), and γ-$[Mn(dpt24)_2]\cdot g$ (**3c**$\cdot$g, g = toluene and MeOH). Their structures were characterized by single-crystal and powder X-ray diffractions. In these compounds, four coordination sites of each octahedrally coordinated Mn^{II} ion are chelated by two dpt24 ligands in the *trans* and/or *cis* configurations. While the two remaining coordination sites are occupied by solvent molecules in **1** and **2**, they are occupied by pyridyl nitrogens from neighboring $Mn(dpt24)_2$ units in **3**, forming 4-connected 2D (4,4) networks. The Mn^{II} ions in both **3a** and **3b** are uniquely chelated by dpt24 in the *trans* or *cis* configurations, respectively, but $Mn(dpt24)_2$ in **3c** possesses both the *trans* and *cis* configurations. The packing fashions of these (4,4) layers in the three isomers of **3** are also different, in which **3a** has a close packing structure, while **3b** exhibits unique one-dimensional (1D) channels and **3c** exhibits two distinct types of 1D channels. As revealed by powder X-ray diffractions, crystals of **1** and **2** can reversibly transform to each other when in contact with the corresponding solvent vapor (H_2O/MeOH). The gas and vapor sorption studies for porous **3b** revealed interesting sorption behaviors. Nitrogen adsorption for **3b** was observed at 195 K rather than 77 K, demonstrating the temperature-controlled framework flexibility. It also exhibited high selectivity and storage capacity for carbon dioxide over methane and nitrogen at room temperature. Moreover, **3b** also demonstrated potential to separate organic chemicals with similar boiling points, such as benzene and cyclohexane, via pressure swing adsorption process.

Introduction

Porous coordination polymers (PCPs) have attracted much attention recently on account of their exceptional adsorption properties. Highly robust and open frameworks that could overcome the problem of collapse after guest removal and show permanent porosity have been the major research goal in the past decade.[1] Recently, designable functionalities of the pore surfaces have been emerging as a topical strategy. Introduction of coordinatively unsaturated metal sites and functional organic sites has been demonstrated to be beneficial for catalysis and adsorption.[2−7] On the other hand, flexible PCPs which could adsorb size-targeted guest molecules by expanding, contracting, and distorting their host frameworks have been recognized as an advantage for high-performance molecular separation, recognition, and sensing applications.[8−12] Obviously, these approaches rely on the rational construction of PCPs.

However, structural uncertainty is an intrinsic problem in the syntheses of coordination polymers, as one can hardly predict the chemical composition of a coordination polymer

*To whom correspondence should be addressed. E-mail: zhangjp7@mail.sysu.edu.cn (J.-P.Z.), cxm@mail.sysu.edu.cn (X.-M.C.). Fax: +86 20 8411-2245.

(1) Yaghi, O. M.; O'Keeffe, M.; Ockwig, N. W.; Chae, H. K.; Eddaoudi, M.; Kim, J. *Nature* **2003**, *423*, 705.
(2) Kitagawa, S.; Noro, S.; Nakamura, T. *Chem. Commun.* **2006**, 701.
(3) Collins, D. J.; Zhou, H. C. *J. Mater. Chem.* **2007**, *17*, 3154.
(4) Dinca, M.; Long, J. R. *Angew. Chem., Int. Ed.* **2008**, *47*, 6766.
(5) Hwang, Y. K.; Hong, D.-Y.; Chang, J.-S.; Jhung, S. H.; Seo, Y.-K.; Kim, J.; Vimont, A.; Daturi, M.; Serre, C.; Férey, G. *Angew. Chem., Int. Ed.* **2008**, *47*, 4144.
(6) Horike, S.; Dinca, M.; Tamaki, K.; Long, J. R. *J. Am. Chem. Soc.* **2008**, *130*, 5854.
(7) Hasegawa, S.; Horike, S.; Matsuda, R.; Furukawa, S.; Mochizuki, K.; Kinoshita, Y.; Kitagawa, S. *J. Am. Chem. Soc.* **2007**, *129*, 2607.
(8) Kitagawa, S.; Kitaura, R.; Noro, S. *Angew. Chem., Int. Ed.* **2004**, *43*, 2334.
(9) Kitagawa, S.; Uemura, K. *Chem. Soc. Rev.* **2005**, *34*, 109.
(10) Bradshaw, D.; Claridge, J. B.; Cussen, E. J.; Prior, T. J.; Rosseinsky, M. J. *Acc. Chem. Res.* **2005**, *38*, 273.
(11) Kepert, C. J. *Chem. Commun.* **2006**, 695.
(12) Férey, G. *Chem. Soc. Rev.* **2008**, *37*, 191.

 Published on Web 06/15/2009

Scheme 1. Possible Coordination Modes of dpt22, dpt44, and dpt24[a]

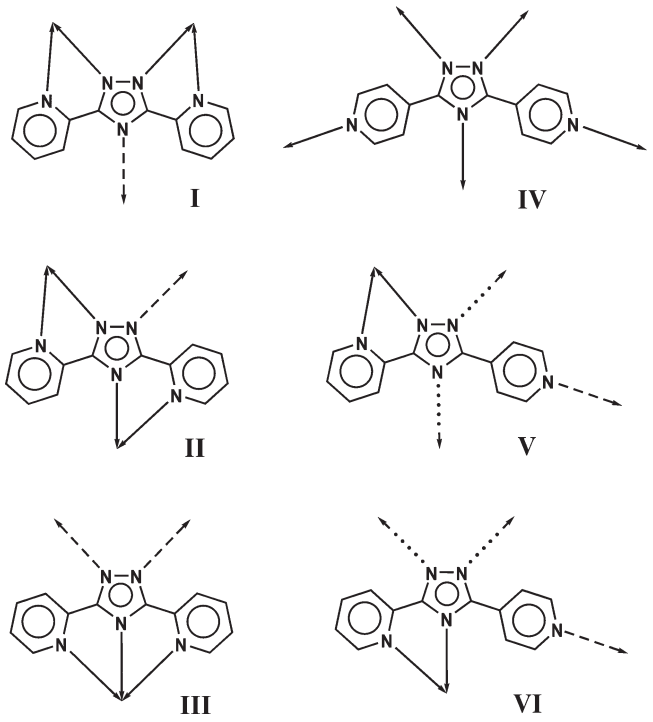

[a] Lined, dashed, and dotted arrows represent primary, secondary, and tertiary coordination sites, respectively.

for a given reaction. Even for a fixed chemical composition, structural diversity or supramolecular isomerism remains another common phenomenon. Actually, supramolecular isomerism should not be simply considered as a problem or challenge, but an opportunity for understanding self-assembly and crystallization processes. Furthermore, supramolecular isomerism in coordination polymers would also benefit the fabrication of multifunctional materials and the understanding of the relationship between supramolecular structures and properties.

To study the above-mentioned issues, we have been devoted to an interesting subset of coordination polymers, namely, metal-azolate frameworks (MAFs).[13] When azolate ligands are coordinated with transition metal ions with appropriate coordination numbers and positive charge, highly insoluble, neutral MAFs such as $M^{I}A$ and $M^{II}A_2$ (A denotes diazolates and triazolates) can readily precipitate. Consequently, these MAFs are good candidates for the studies of supramolecular isomerism and construction of coordination polymers with diverse structure and properties.

To rationally construct new porous MAFs, we have designed a new multidentate azolate ligand, 3-(2-pyridyl)-5-(4-pyridyl)-1,2,4-triazole (Hdpt24), which is an unsymmetrical isomer of 3,5-di-(2-pyridyl)-1,2,4-triazole (Hdpt22) and 3,5-di-(4-pyridyl)-1,2,4-triazole (Hdpt44).[14,15] As shown in Scheme 1, the coordination behaviors of these azolates, dpt24, dpt22, and dpt44, are remarkably different. Because

Scheme 2. $M(dpt24)_2L_2$ in *trans* and *cis* Configurations[a]

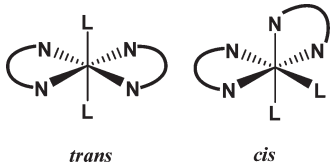

[a] L represents auxiliary ligand.

of the rotational flexibility of 2-pyridyl groups, dpt22 exhibits three major conformations. Two of them possess two bidentate chelating sites and a monodentate one (I and II), while the third one bears a tridentate chelating site and two monodentate ones (III). We could easily predict the coordination mode and chemical composition for the Cu^{I}-dpt22 system to synthesize a series of supramolecular isomers, since tetrahedrally coordinated Cu^{I} is appropriate for two bidentate chelating.[14] However, dpt44 has five potential monodentate sites (IV). It is hard to predict the local coordination environments and superstructures of its MAFs, although several supramolecular isomers had been isolated for the [Cu(dpt44)] system.[15] The new ligand dpt24 exhibits two conformations dependent on the orientation of the 2-pyridyl group (V and VI), both possess a bidentate chelating site and three monodentate sites. When dpt24 is coordinated with a metal ion, it would first use the bidentate chelating site and then use other monodentate ones. Because of steric hindrance effects, the pyridyl nitrogen has a higher priority in coordination than the remaining azolate nitrogens. When a divalent metal ion is used, the metal ion should be chelated by two dpt24 ligands to give a neutral $M(dpt24)_2$ unit, for a divalent metal ion prefers a common octahedral coordination mode; the two remaining sites should be occupied by other ligands. Depending on the reaction mediums and conditions, these two sites can be occupied by auxiliary terminal ligands (L) to give a discrete mononuclear complex $[M(dpt24)_2L_2]$, or by the nitrogen donors from two other $M(dpt24)_2$ units to give a 4-connected coordination polymer $[M(dpt24)_2]$ (each metal ion is coordinated by four dpt24 and each dpt24 is coordinated to two metal ions). If dpt24 uses the pyridyl nitrogen to link another metal ion, the separations between two adjacent metal centers are larger than 8 Å, which is useful for the construction of open frameworks. Meanwhile, the two uncoordinated triazolate nitrogens would be exposed on the pore surfaces as guest-accessible sites for catalysis or adsorption. The lone pair electrons of uncoordinated nitrogens would be also useful for interacting with gas molecules such as CO_2, whose carbon atom acts as an electron-acceptor.[16−19] On the other hand, an octahedral metal ion chelated by two bidentate ligands could exhibit stereoisomerism by forming the *trans* or *cis* configuration (Scheme 2). In this context, $[M(dpt24)_2]$ is a promising candidate for construct PCPs with basic pore surface and structural diversity.

Our hypotheses have now been confirmed through reactions of Hdpt24 with $Mn(OAc)_2$ under different

(13) For recent example, see: Lin, Y.-Y.; Zhang, Y.-B.; Zhang, J.-P.; Chen, X.-M. *Cryst. Growth Des.* **2008**, *8*, 3673.
(14) Zhang, J.-P.; Lin, Y.-Y.; Huang, X.-C.; Chen, X.-M. *Chem. Commun.* **2005**, 1258.
(15) Zhang, J.-P.; Lin, Y.-Y.; Huang, X.-C.; Chen, X.-M. *Cryst. Growth Des.* **2006**, *6*, 519.
(16) Vimont, A.; Travert, A.; Bazin, P.; Lavalley, J. C.; Daturi, M.; Serre, C.; Férey, G.; Bourrelly, S.; Llewellyn, P. L. *Chem. Commun.* **2007**, 3291.
(17) Meredith, J. C.; Johnston, K. P.; Seminario, J. M.; Kazarian, S. G.; Eckert, C. A. *J. Phys. Chem.* **1996**, *100*, 10837.
(18) Kazarian, S. G.; Vincent, M. F.; Bright, F. V.; Liotta, C. L.; Eckert, C. A. *J. Am. Chem. Soc.* **1996**, *118*, 1729.
(19) Danten, Y.; Tassaing, T.; Besnard, M. *J. Phys. Chem. A* **2002**, *106*, 11831.

conditions, which produce a series of new coordination complexes, including two mononuclear complexes [Mn(dpt24)$_2$(MeOH)$_2$] (**1**) and [Mn(dpt24)$_2$(H$_2$O)$_2$]·6H$_2$O (**2**), and three isomeric MAFs α-[Mn(dpt24)$_2$] (MAF-24α, **3a**), β-[Mn(dpt24)$_2$]·g (MAF-24β, **3b**·g, g = DMF and H$_2$O), and γ-[Mn(dpt24)$_2$]·g (MAF-24γ, **3c**·g, g = toluene and MeOH). In addition to the controlled self-assembly and rich structural diversity, **1** and **2** exhibit interesting, reversible solid-state transformations between each other, and isomers of **3** show different sorption properties dependent on their superstructures.

Experimental Section

Materials and Methods. Commercially available reagents were used as received without further purification. Hdpt24 was prepared according to a reported method.[20] Elemental analyses (C, H, N) were performed on a Perkin-Elmer 240 elemental analyzer. The FT-IR (KBr pellet) spectra were recorded from KBr pellets in the range of 400−4000 cm^{-1} on a Bruker TENSOR 27 FT-IR spectrometer. Thermal gravimetric analysis was performed under N$_2$ using a NETZSCH TG 209 system. Powder X-ray diffraction (PXRD) patterns were recorded on a Bruker D8 Advance diffractometer or a Rigaku D/M-2200T automated diffractometer (Cu Kα). Gas sorption isotherms were measured on a volumetric adsorption apparatus (Bel-max). Solvent vapor isotherms were measured on an automatic gravimetric adsorption apparatus (IGA-003 series, Hiden Isochema Ltd.).

Synthesis of [Mn(dpt24)$_2$(CH$_3$OH)$_2$] (1). Hdpt24 (0.112 g, 0.5 mmol) was refluxed in the mixed solution of DMF (4 mL) and MeOH (5 mL) to yield a clear solution. The solution was then added into a MeOH solution (4 mL) of Mn(OAc)$_2$·4H$_2$O (0.061 g, 0.25 mmol). After the resulting solution was placed in a silicagel desiccator for several days, yellow crystals of **1** were isolated in about 50% yield based on Mn. When the filtrate was further stirred for 1 day, powder product of **1** was obtained. Anal. Calcd (%) for C$_{26}$H$_{24}$MnN$_{10}$O$_2$: C, 55.42; H, 4.29; N, 24.86. Found: C, 54.86; H, 4.06; N, 25.17. IR: 3410m, 1655w, 1605vs, 1506m, 1425m, 1169w, 1105w, 1059w, 999m, 837m, 795m, 737s, 696m, 644m, 505w, 422w cm^{-1}.

Synthesis of [Mn(dpt24)$_2$(H$_2$O)$_2$]·6H$_2$O (2). Hdpt24 (0.112 g, 0.5 mmol) was refluxed in DMF (10 mL) to give a clear solution, to which a H$_2$O solution (10 mL) of Mn(OAc)$_2$·4H$_2$O (0.061 g, 0.25 mmol) was added. After the resulting solution was placed in a silicagel desiccator for several days, pale-yellow crystals of **2** were isolated in about 47% yield based on Mn. When a DMF solution of Hdpt24 was added into a water solution of Mn(OAc)$_2$·4H$_2$O and stirred for 1 hr, powder product of **2** was obtained. Anal. Calcd (%) for C$_{24}$H$_{32}$MnN$_{10}$O$_8$: C, 44.79; H, 5.01; N, 21.77. Found: C, 44.67; H, 4.96; N, 21.80. IR: 3422m, 1645w, 1607vs, 1568w, 1510w, 1427s, 1171w, 1013w, 837w, 795w, 741s, 698w, 638w, 424w cm^{-1}.

Synthesis of α-[Mn(dpt24)$_2$] (3a). A mixture of Mn(OAc)$_2$·4H$_2$O (0.061 g, 0.25 mmol), Hdpt24 (0.112 g, 0.5 mmol), and MeCN (4 mL) was sealed in a 15 mL Teflon-lined reactor and heated at 190 °C for 3 days, and then cooled by 5 °C/h to room temperature. The product was a mixture while a few pale-yellow crystals of **3a** suitable for single-crystal X-ray diffraction were mechanically isolated. IR: 3832w, 3736w, 3363vs, 1606vs, 1566s, 1512s, 1425s, 1169m, 1106w, 1011m, 836w, 737s, 637m cm^{-1}.

Synthesis of β-[Mn(dpt24)$_2$]·g (3b·g). Method A. A mixture of Mn(OAc)$_2$·4H$_2$O (0.061 g, 0.25 mmol), Hdpt24 (0.112 g, 0.5 mmol), EtOH (2.0 mL), and DMF (4.0 mL) was sealed in a 10 mL Teflon-lined reactor, heated at 160 °C for 4 days and then cooled to room temperature at a rate of 5 °C/h. The resulting clear solution was evaporated for **2** months at room temperature to produce yellowish crystals of **3b**·0.5DMF·3H$_2$O in about 35% yield based on Mn. Anal. Calcd (%) for [Mn(dpt24)$_2$]·0.5DMF·3H$_2$O (C$_{25.5}$H$_{25.5}$MnN$_{10.5}$O$_{3.5}$): C, 51.91; H, 4.36; N, 24.93. Found: C, 51.32; H, 4.45; N, 24.63. IR: 3439s, 3072w, 2032w, 1659m, 1607vs, 1456s, 1418m, 1153m, 1099w, 1009m, 912w, 841m, 800m, 741s, 692w, 629w, 548w, 494w cm^{-1}.

Method B. Large amounts of **3b**·g were obtained by the following procedure. A mixture of Mn(OAc)$_2$·4H$_2$O (0.061 g, 0.25 mmol), Hdpt24 (0.112 g, 0.5 mmol), EtOH (5.0 mL), and DMF (0.2 mL) was sealed in a 15 mL Teflon-lined reactor, heated at 160 °C for 3 days, and then cooled to room temperature at a rate of 5 °C/h. The resulting precipitate was washed with ethanol, and dried in air to give yellow powders of **3b**·3.5H$_2$O in about 48% yield based on Mn. Anal. Calcd (%) for [Mn(dpt24)$_2$]·3.5H$_2$O (C$_{24}$H$_{23}$MnN$_{10}$O$_{3.5}$): C, 51.25; H, 4.12; N, 24.90. Found: C, 50.43; H, 4.16; N, 25.60. IR: 3848w, 3830w, 3746w, 3680w, 3439s, 1610vs, 1568w, 1512w, 1427m, 1389w, 1101w, 1059w, 1013w, 847w, 741m, 696w, 419w cm^{-1}.

Synthesis of γ-[Mn(dpt24)$_2$]·0.5C$_7$H$_8$·1.5CH$_3$OH (3c·g). A mixture of Mn(OAc)$_2$·4H$_2$O (0.061 g, 0.25 mmol), Hdpt24 (0.112 g, 0.5 mmol), MeOH (4 mL), and toluene (1 mL) was sealed in a 15 mL Teflon-lined reactor, heated at 160 °C for 4 days, and then cooled to room temperature at a rate of 5 °C/h. Large yellowish crystals of **3c**·0.5C$_7$H$_8$·1.5MeOH were isolated in about 63% yield based on Mn. A satisfactory elemental analysis is not available for the as-synthesized sample since it easily loses some guest molecules after filtration. Alternatively, elemental analysis was carried out for the degassed sample. Anal. Calcd (%) for desolvated [Mn(dpt24)$_2$]: C, 57.72; H, 3.23; N, 28.05. Found: C, 57.36; H, 3.30; N, 27.83. IR: 3412m, 1609vs, 1566w, 1508m, 1427m, 1165w, 1103w, 1013m, 845w, 739s, 696w cm^{-1}.

Crystal Structure Determination. The intensity data were collected on a Bruker Apex CCD area-detector diffractometer (Mo Kα). Absorption corrections were applied by using multiscan program SADABS.[21] The structures were solved with direct methods and refined with a full-matrix least-squares technique with the SHELXTL program package.[22] Anisotropic thermal parameters were applied to all non-hydrogen atoms except the guest molecules. The organic hydrogen atoms were generated geometrically. Crystal data and refinement parameters for the complexes are summarized in Table 1. Selected bond lengths and angles are given in Supporting Information, Table S1.

Results and Discussion

Crystal Structures. The molecular structure of **1** is shown in Figure 1a. The Mn^{II} ion, being located at an inversion center, displays a distorted octahedral coordination geometry by coordination with four nitrogens from two dpt24 in mode V and two MeOH oxygens. The Mn−N(2-pyridyl) bond length (2.250(2) Å) is slightly longer than the Mn−N(azolate) bond (2.171(2) Å) but equals that of the Mn−O bond (2.250(2) Å).

Each uncoordinated triazolate 4-nitrogen of **1** is hydrogen-bonded by a hydroxyl group of MeOH from a neighboring molecule [O···N 2.744(3) Å], forming a two-dimensional (2D) layer in the *bc* plane (Figure 1b). Further, each uncoordinated pyridine nitrogen is hydrogen-bonded by a pyridyl C−H moiety from a neighboring molecule [C···N 3.466(5) Å], forming a three-dimensional (3D) architecture (Figure 1c).

(20) Browne, E. J. *Aust. J. Chem.* **1975**, *28*, 2543.

(21) Sheldrick, G. M. *SADABS 2.05*; University Göttingen: Göttingen, Germany, 2002.

(22) *SHELXTL 6.12*; Bruker Analytical Instrumentation: Madison, WI, 2000.

Table 1. Crystallographic Data

complex	**1**	**2**	**3a**	**3b**	**3c**
formula	$C_{26}H_{24}MnN_{10}O_2$	$C_{24}H_{32}MnN_{10}O_8$	$C_{24}H_{16}MnN_{10}$	$C_{25.5}H_{25.5}MnN_{10.5}O_{3.5}$	$C_{29}H_{26}MnN_{10}O_{1.5}$
formula weight	563.49	643.54	499.41	590.00	593.54
crystal system	monoclinic	orthorhombic	monoclinic	tetragonal	monoclinic
space group	$P2_1/c$ (No. 14)	*Pbcn* (No. 60)	$P2_1/n$ (No. 14)	$P4_2/n$ (No. 86)	$P2_1/c$ (No. 14)
a/Å	10.873(3)	17.951(6)	8.800(2)	13.7675(8)	26.242(3)
b/Å	12.902(4)	8.001(3)	14.920(3)	13.7675(8)	14.332(2)
c/Å	10.039(3)	20.889(7)	9.377(2)	14.543(2)	15.204(2)
β/deg	113.297(5)	90	108.615(4)	90	106.611(2)
V/Å^3	1293.5(7)	3000 (2)	1166.7(4)	2756.5(4)	5480(1)
Z	2	4	2	4	8
D_c /g cm^{-3}	1.447	1.425	1.422	1.422	1.439
μ/mm^{-1}	0.556	0.503	0.600	0.529	0.528
reflns coll.	4788	10428	5483	10441	28846
unique reflns	2516	2940	2284	2677	10261
R_{int}	0.0292	0.0297	0.0468	0.0613	0.0768
R_1 $[I > 2\sigma(I)]^a$	0.0551	0.0389	0.0788	0.0813	0.0673
wR_2 $[I > 2\sigma(I)]^b$	0.1271	0.1034	0.2216	0.2008	0.1808
R_1 (all data)	0.0708	0.0489	0.0977	0.1205	0.1011
wR_2 (all data)	0.1366	0.1125	0.2391	0.2250	0.2098
GOF	1.053	1.002	1.005	1.065	1.043
$\Delta\rho_{min/max}$/e/Å^3	0.326/−0.302	0.300/−0.203	0.531/−0.716	0.835/−0.424	0.787/−0.495

$^a R_1 = \sum||F_o| - |F_c||/\sum|F_o|$. $^b wR_2 = [\sum w(F_o^2 - F_c^2)^2/\sum w(F_o^2)^2]^{1/2}$.

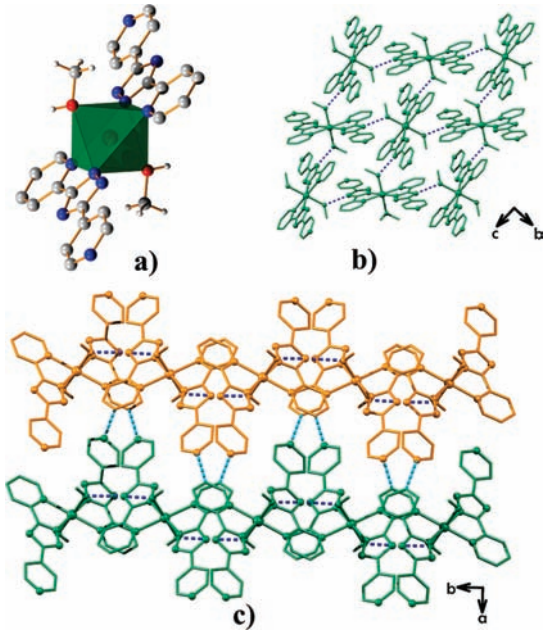

Figure 1. (a) Coordination environment of the Mn^{II} ion, (b) hydrogen-bonded layer, and (c) hydrogen-bonded 3D structure of **1**.

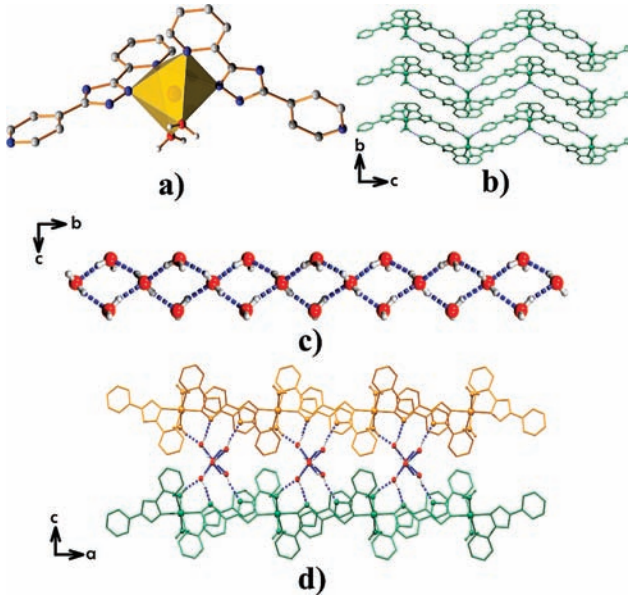

Figure 2. (a) Coordination environment of the Mn^{II} ion, (b) hydrogen-bonded chain, (c) T4(1) lattice water tape, and (d) hydrogen-bonded 3D structure of **2**.

In **2**, the Mn^{II} ion, being located at a 2-fold axis, is also coordinated by four nitrogens from two dpt24 in mode V and two aqua oxygens in a distorted octahedral N_4O_2 geometry (Figure 2a). The Mn−O bond (2.153(2) Å) is shorter than the Mn−N bonds (2.195(2) and 2.311(2) Å). Different from the trans configuration of **1**, two aqua oxygens in **2** occupy the cis positions (O−Mn−O 90.6 (1)°).

Each uncoordinated pyridyl nitrogen of **2** is hydrogen-bonded by an aqua ligand of a neighboring molecule [O···N 2.701(2) Å], forming a unique zigzag ladder-type structure along the *c*-axis (Figure 2b). The lattice water molecules among these chains are hydrogen-bonded by each other to form T4(1) tapes (O···O 2.709(3)−2.821(3) Å) along the *b*-axis (Figure 2c).[23] Each uncoordinated nitrogen of the triazolato ring and coordinated aqua oxygen are hydrogen-bonded by the T4(1) lattice water tape (O···N3 2.729(2), O···N4 2.820(3), O···O 2.714(2) Å) to furnish a 3D architecture (Figure 2d).

All Mn^{II} ions in **3** are also chelated by two dpt24 ligands in mode V. However, the two remaining coordination sites of each Mn^{II} ion in **3** are coordinated by 4-pyridyl nitrogens from adjacent $Mn(dpt24)_2$ units, giving rise to polymeric structures.

(23) Infantes, L.; Motherwell, S. *CrystEngComm* **2002**, 454.

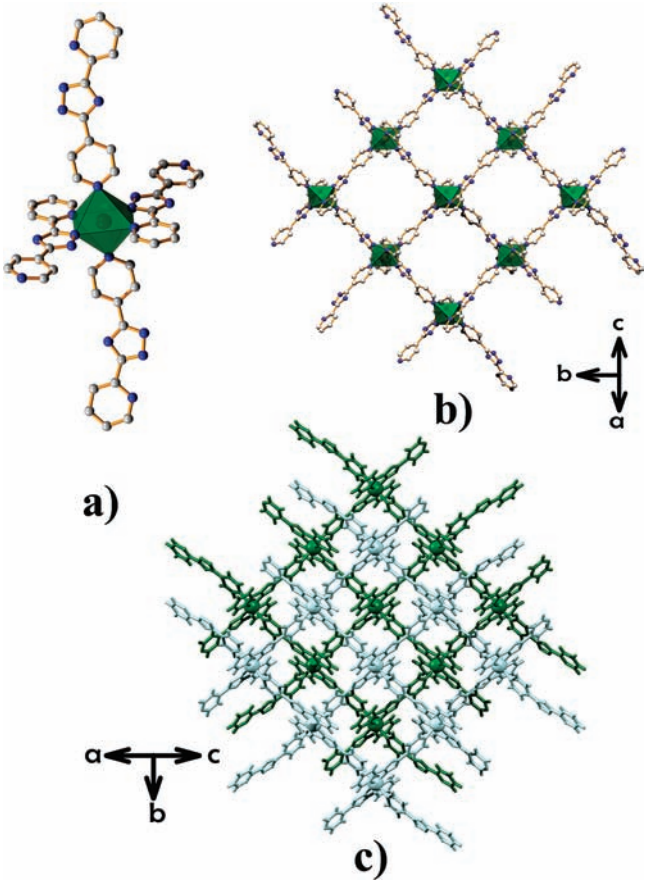

Figure 3. (a) Coordination environment of the Mn^{II} ion and dpt24, (b) (4,4) network layer, and (c) layer stacking in **3a**.

In **3a**, the Mn^{II} ion located at an inversion center is coordinated in a distorted octahedral N_6 coordination environment (Mn−N 2.152(4)−2.352(4) Å) (Figure 3a). Each $Mn(dpt24)_2$ fragment is linked by two 4-pyridyl nitrogens from two neighboring $Mn(dpt24)_2$ fragments, forming 2D square-grid sheets (Mn···Mn squares 10.50 × 10.50 $Å^2$; Figure 3b), which stack along the [506] direction in an staggered fashion (Figure 3c) with interlayer $\pi-\pi$ stacking interactions (3.5−3.6 Å) between phenyl and/or triazolate planes and C−H···N hydrogen-bonds (3.3−3.6 Å), leading to a 3D close packing structure. Although there is 7.6% void volume in **3a** as calculated by Platon,[24] the discrete cages are isolated from each other and inaccessible to guest molecules (Supporting Information, Figure S1).

Depending on the synthetic method, **3b** can contain different guests. The DMF-H_2O solvate of **3b** is suitable for crystallographic analysis. Isomer **3b** exhibits a 2D square-grid structure (Mn···Mn square 10.32 × 10.32 $Å^2$) constructed by *cis*-$Mn(dpt24)_2$ units (Mn−N 2.221(4)−2.312(4) Å; Figure 4a,b). Because of the *cis* configuration of $Mn(dpt24)_2$, two kinds of squares with the same side length exist in the 2D layer in **3b**. Among them, one is surrounded by four triazolate 4-nitrogens, and the other is enclosed by four triazolate 2-nitrogens. Although the (4,4) networks stack along the *c*-axis in an offset fashion (interlayer $\pi-\pi$ separations between triazolate planes are 3.6 Å), two kinds of squares are stacked

(24) Spek, A. L. *J. Appl. Crystallogr.* **2003**, *36*, 7.

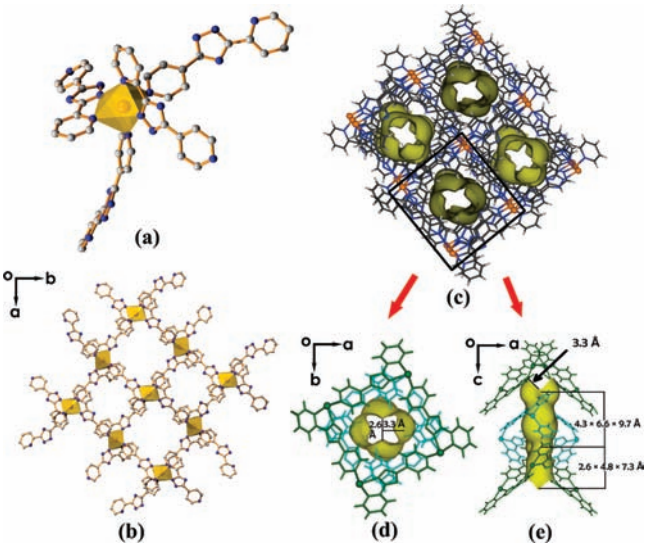

Figure 4. (a) Coordination environment of the Mn^{II} ion and dpt24, (b) (4,4) layer, (c) 3D stacking structure, and the (d) top- and (e) side-views of the channels of **3b**.

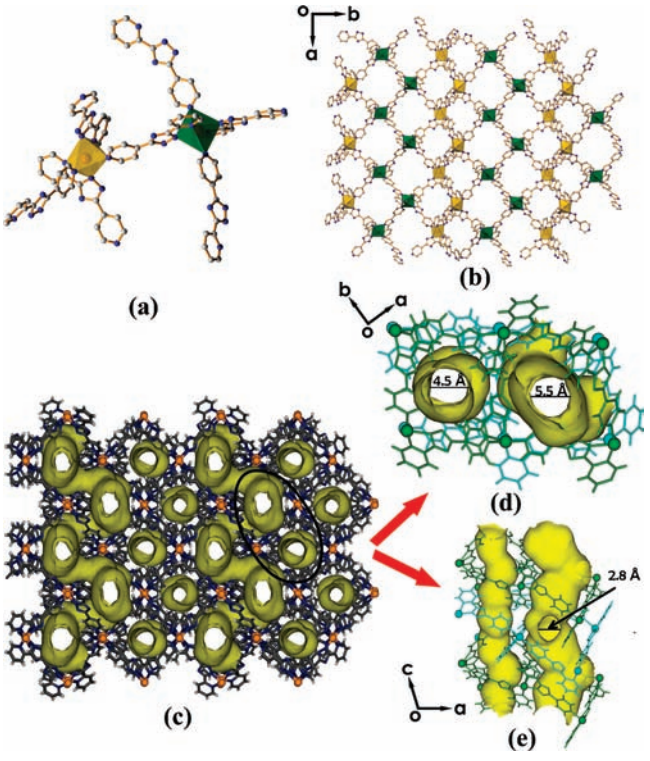

Figure 5. (a) Coordination environments of Mn^{II} ions and dpt24, (b) (4,4) layer, (c) 3D stacking structure, and the (d) top- and (e) side-views of the channels of **3c**.

alternately. Consequently, there is a unique type of one-dimensional (1D) channel running along the *c*-axis (Figure 4c), and the channel is generated by interconnection of two kinds of cavities with different sizes and shapes (ca. 4.3 × 6.6 × 9.7 and 2.6 × 4.8 × 7.3 $Å^3$), where two smallest cross-section size of entrances (3.3 Å) are overlapped in a peanut-like shape (Figure 4d,e). Lattice H_2O and disordered DMF guest molecules occupy 25.3% volume of **3b**.[24] The uncoordinated triazolate 4-nitrogens as functional sites are exposed inside the channel, which

are hydrogen-bonded by the lattice water molecules (O···N 2.903(7) Å).

In **3c**, each asymmetric unit contains two Mn^{II} ions and four dpt24 ligands. As shown in Figure 5a, Mn1 and Mn2 are each coordinated by two dpt24 ligands in a *trans* or *cis* configuration (Mn−N 2.181(3)−2.310(4) Å), respectively. Because of the presence of two types of stereo configurations, two kinds of quadrilaterals are generated, as shown in Figure 5b. One quadrilateral is planar with Mn···Mn distances of 10.62, 10.62, 10.64, and 10.47 Å, while the other one is bent with Mn···Mn distances of 10.30, 10.30, 10.64, and 10.47 Å. The 2D layers stack along the *c*-axis in an offset fashion with interlayer $\pi-\pi$ interactions (3.3−3.7 Å) between pyridyl groups and C−H···N hydrogen-bonds (2.9−3.4 Å) to give a 3D structure. 26.9% volume[24] of **3c** (Figure 5c) is occupied by the guest solvent molecules MeOH and toluene. The smallest sizes of the cross-section of two different channels are about 4.5 and 5.5 Å (Figure 5d), respectively. The smaller channel is filled with MeOH molecules, and the larger one contains toluene and MeOH molecules. Furthermore, the larger channels are linked by small passages (ca. 2.8 Å) (Figure 5e) to a 2D channel system in the *bc* plane. The uncoordinated triazolate 4-nitrogens, which are hydrogen-bonded by hydroxyl group of MeOH (O···N 2.772(5) and 2.824(5) Å), are also exposed inside the channel.

Syntheses. As accurate prediction of the final product of self-assembly and crystallization is intrinsically difficult, we have tried different synthetic routes to study the possible coordination behaviors of the new MAF system. Five coordination complexes were isolated by varying solvent, temperature, and reactant concentration. It should be noted that, all five complexes exhibit the predicted neutral 1:2 Mn^{II}-dpt24 stoichiometry, and the coordination modes of dpt24 ligands are all in mode V. The absence of mode VI for dpt24 might be ascribed to the steric hindrance effect of the 4-pyridyl ring (hydrogen atom). Moreover, rich structural diversity and supramolecular isomerism were developed by the existence of *cis* and *trans* stereo configuration for the $Mn(dpt24)_2$ centers. These observations indicate that rational construction of coordination complexes and supramolecular isomers can be achieved by judicious design of organic ligands.

Although the exact rules of synthetic conditions in directing the structures can be hardly explained (representative synthetic routes were shown in Scheme 3), we have observed some general relations. Compared to the polymeric structures **3**, mononuclear complexes **1** and **2** prefer to crystallize at lower temperature and shorter reaction time. For instance, by vigorous stirring the clear solution, powders of **1** and **2** could rapidly precipitate at room temperature.

As the isomeric structures of **3** are the inclusion of different guest molecules, they can be categorized as guest-induced isomerism. Close packing **3a** was produced in the pure aprotic solvent MeCN. When protic solvents (MeOH or EtOH) were introduced, porous **3b** and **3c** were generated. It is reasonable to conclude that aprotic solvent molecules alone can hardly form hydrogen bonds to the uncoordinated triazolato nitrogens and then behave as a template. Nevertheless, aprotic solvent

Scheme 3. Syntheses and Transformations for **1**−**3**

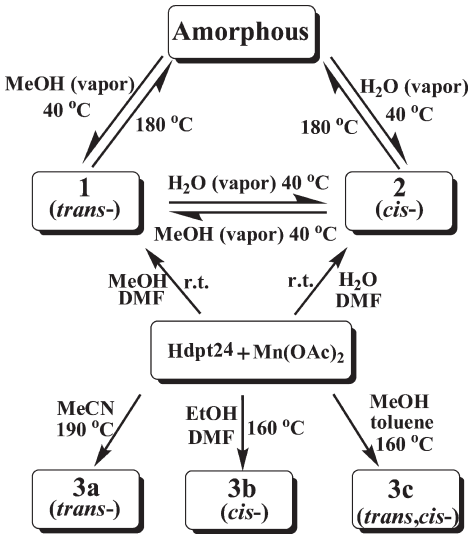

molecules can act as a co-template in the presence of protic solvent molecules. Consequently, different porous structures can be templated by alteration of a variety of solvents. For example, **3b** and **3c** were obtained in DMF/EtOH and toluene/MeOH, respectively. On the basis of the rich structural diversity of this MAF, more potential isomers of **3** would be synthesized in suitable reaction conditions, if found. Generally, the isolation of certain products rather than other potential ones should be due to their relatively high stabilities or low framework energies. This principle is illustrated by the fact that **1**−**3** can tolerate a certain variation of reaction conditions. For example, the single-crystal of $\mathbf{3b}\cdot 0.5DMF\cdot 3H_2O$ could be generated by evaporation of the solvothermally treated ethanol-DMF solution at room temperature, while powders of $\mathbf{3b}\cdot 3.5H_2O$ were obtained in higher yield by direct solvothermal reaction with a lower DMF concentration.

Structural Transformation. Considering the short distance (ca. 2.7 Å) between coordinated oxygen and uncoordinated nitrogen from neighboring $[Mn(dpt24)_2L_2]$ molecules, $Mn(dpt24)_2$ units in **1** and **2** may be interconnected by the uncoordinated nitrogen donors into higher dimensional structures after the removal of auxiliary terminal ligands.[25] Therefore, we have studied their structural transformation by heating. Unfortunately, both **1** and **2** were changed to amorphous structures after loss of the coordinated solvent molecules (Supporting Information, Figures S2 and S3). However, these amorphous $[Mn(dpt24)_2]$, either obtained from **1** or **2**, could be converted to crystalline **1** or **2** in contact with a MeOH or H_2O vapor, respectively (Scheme 3 and Supporting Information, Figure S2). Presumably, after the coordinated solvent molecules are removed, Mn^{II} ions are in $Mn^{II}N_4$ tetrahedral and/or $Mn^{II}N_6$ octahedral coordination geometries because the original $Mn^{II}N_4$ geometries, both in *cis* and *trans* $Mn^{II}N_4L_2$, are not stable after the removal of two L and generation of two vacant sites.[26] The amorphous structures of

(25) Cheng, X.-N.; Zhang, W.-X.; Chen, X.-M. *J. Am. Chem. Soc.* **2007**, *129*, 15738.

(26) Cambridge Structrual Database V5.29, Copyright CCDC **2008**.

$[Mn(dpt24)_2]$ imply that the Mn centers are not strongly interconnected, which can be explained by the formation of randomly located $[Mn(dpt24)_2]$ molecules and/or partial/weak intermolecular connection. When the desolvated compound is exposed in the solvent vapor, the solvent molecules will attack the tetrahedral and/or weakly ligated octahedral sites, resulting in the corresponding solvated structure. Assuming there is certain octahedral coordinated Mn^{II} presented in the amorphous $[Mn(dpt24)_2]$, the configuration of $[Mn(dpt24)_2L_2]$ should be strongly determined by auxiliary solvent ligands rather than the $[Mn(dpt24)_2]$ precursors. Moreover, direct solid-state interconversions between **1** and **2** were also observed (Scheme 3 and Supporting Information, Figure S2). The crystal-to-crystal transformation is reversible by exposing **1** in H_2O vapor or **2** in MeOH vapor. This phenomenon confirms the above speculation and implies that the single coordination bonds between Mn^{II} and solvent molecules are rather labile. Therefore, discrete **1** and **2** are stable at relatively low temperatures while polymeric **3** prefer higher temperatures. The reversible crystal-to-crystal and crystal-to-amorphous interconversions between **1** and **2** are novel as they involve breakage and formation of coordination and hydrogen bonds, *trans-cis* conversion of stereo configuration, and rearrangement of molecules in the crystal lattices,[27] though *trans-cis* conversion of metal complexes have been studied extensively by adsorption spectroscopy in solution or solid state.[28−34]

Thermal Stability. **3b**·0.5DMF·$3H_2O$ shows a slow weight loss of DMF and H_2O molecules below 240 °C (observed: 16.8%, calculated: 15.4%), and no further weight loss below 400 °C until decomposition. **3b**·$3.5H_2O$ shows rapid weight loss of water molecules below 120 °C (observed 10.9%, calculated 11.2%), and decomposes after 400 °C (Supporting Information, Figure S4). However, the high temperature PXRD analyses reveal that crystal structures of **3b** can only be retained up to 300 °C (Supporting Information, Figure S5), which may be ascribed to the relatively weak Mn^{II}-pyridine coordination bonds. TGA of **3c**·$0.5C_7H_8$·1.5MeOH exhibits a weight loss of 14.7% from 30 to 180 °C corresponding to 0.5 toluene and 1.5 MeOH molecules per $Mn(dpt24)_2$ unit (calculated 15.8%). There is no further weight loss below 420 °C until decomposition (Supporting Information, Figure S4). However, as shown by the PXRD pattern (Supporting Information, Figure S6), desolvated **3c** undergoes an irreversible structural change.

Sorption Properties. The smallest cross-section size of entrances (3.3 Å) estimated by the single-crystal structure of **3b**·g at room temperature is close to the molecular dimensions of CO_2 ($3.2 \times 3.3 \times 5.4$ Å^3, kinetic diameter 3.3 Å) and N_2 ($3.0 \times 3.1 \times 4.0$ Å^3, 3.64 Å) but smaller than that of CH_4 ($3.8 \times 3.9 \times 4.1$ Å^3, 3.8 Å).[35] To examine the pore characteristics and storage capability of the desolvated **3b**, sorption experiments have been performed with CO_2, N_2, CH_4, and different volatile organic molecules.

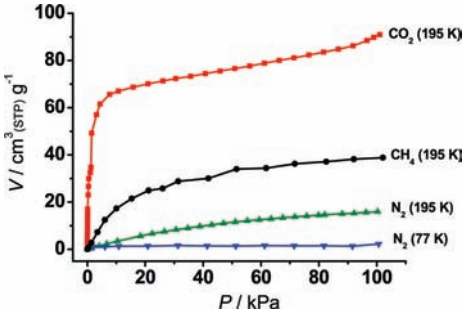

Figure 6. Carbon dioxide, methane, and nitrogen adsorption isotherms for **3b**.

The N_2 adsorption isotherms of dehydrated **3b** were measured at 77 and 195 K (Figure 6). It shows only surface adsorption for N_2 at 77 K (2.2 $cm^3(STP)\cdot g^{-1}$ at P = 101 kPa). However, **3b** can readily adsorb N_2 at 195 K. The adsorption amounts of N_2 at P = 100 kPa and 195 K is about 16 $cm^3(STP)\cdot g^{-1}$, which corresponds to 0.36 N_2 per $Mn(dpt24)_2$ unit, indicating the N_2 molecules are absorbed into the channels of **3b** rather than the particle surface. Since the aperture size of **3b** is close to the dimensions of N_2, this temperature-dependent gate-opening behavior could be derived from permanent or momentary expansion of the smallest slits that allow the diffusion of the guest molecules at higher temperature,[36,37] which is further confirmed by CH_4 sorption at 195 K. The adsorption amount of CH_4 at P = 102 kPa is about 39 $cm^3(STP)\cdot g^{-1}$, which corresponds to 0.87 CH_4 per $Mn(dpt24)_2$ unit. At 195 K, since the static size of aperture is smaller than the dimensions of CH_4, the framework must distort to allow the passage of CH_4 molecules.

The CO_2 sorption of **3b** (Figure 6) measured at 195 K exhibits a type I isotherm with an apparent Langmuir surface area of 444 $m^2\cdot g^{-1}$.[38] The adsorption amount of CO_2 at P = 101 kPa is about 91 $cm^3(STP)\cdot g^{-1}$, which corresponds to 2.0 CO_2 per $Mn(dpt24)_2$ unit.

On the other hand, after removal of guest molecules, **3c** could not retain its original framework structure, but it can still adsorb N_2 and H_2 at 77 K (Supporting Information, Figure S7). Unfortunately, we were failed to obtain a smooth isotherm for **3c** using neither N_2 nor H_2, which suggest some non-stability during the sorption measurements. The non-stability of isotherms should be ascribed to the structure transformation of the sample in the sorption process, which was confirmed by PXRD after gas sorption measurements (Supporting Information, Figure S6).

According to the above phenomena, isomers **3b** and **3c** process not only different superstructures but also remarkably distinct framework stabilities. Because of the high stability of **3b**, which may be of use for practical

(27) Adeyemi, O. G.; Eke, U. B.; Cheng, L.; Cook, L. M.; Billing, D. G.; Mamba, B. B.; Levendis, D. C.; Coville, N. J. *J. Organomet. Chem.* **2004**, *689*, 2207.
(28) LeMay, H. E.Jr.; Bailar, J. C.Jr. *J. Am. Chem. Soc.* **1967**, *89*, 5577.
(29) Ihara, Y.; Fukuda, Y.; Sone, K. *Bull. Chem. Soc. Jpn.* **1986**, *59*, 1825.
(30) Krassowski, D. W.; Nelson, J. H.; Brower, K. R.; Hauenstein, D.; Jacobson, R. A. *Inorg. Chem.* **1988**, *27*, 4294.
(31) Krassowski, D. W.; Reimer, K.; LeMay, H. E.Jr.; Nelson, J. H. *Inorg. Chem.* **1988**, *27*, 4307.
(32) Das, D.; Chaudhuri, N. R.; Ghosh, A. *Polyhedron* **1996**, *15*, 3919.
(33) Ihara, Y.; Sakino, T.; Ishikawa, M.; Koyata, T. *Bull. Chem. Soc. Jpn.* **1997**, *70*, 3025.
(34) Vittal, J. J. *Coord. Chem. Rev.* **2007**, *251*, 1781.
(35) Webster, C. E.; Drago, R. S.; Zerner, M. C. *J. Am. Chem. Soc.* **1998**, *120*, 5509.
(36) Zhang, J.-P.; Chen, X.-M. *J. Am. Chem. Soc.* **2008**, *130*, 6010.
(37) Kim, H.; Samsonenko, D. G.; Yoon, M.; Yoon, J. W.; Hwang, Y. K.; Chang, J. S.; Kim, K. *Chem. Commun.* **2008**, 4697.

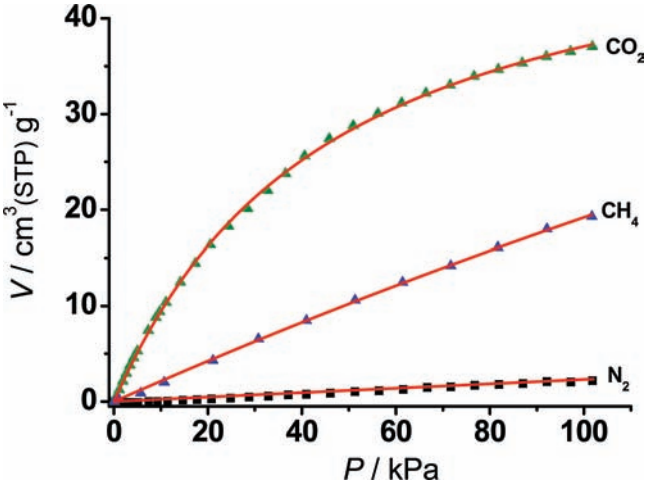

Figure 7. Adsorption isotherms for **3b** measured at 298 K and fitted curves (red lines) based on the Toth isotherm model.

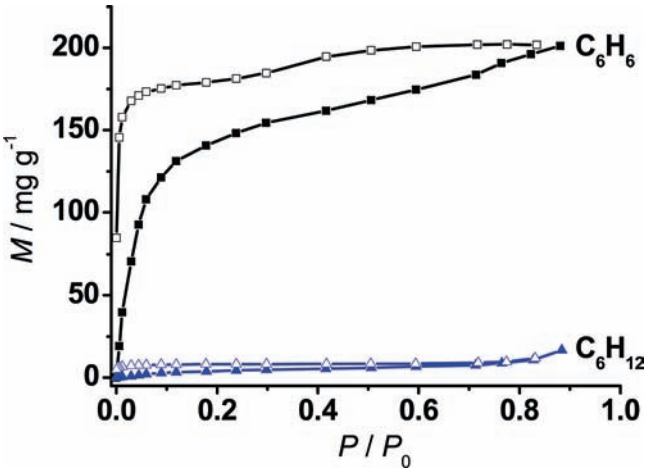

Figure 8. C_6H_6 and C_6H_{12} sorption isotherms for **3b** measured at 298 K (P_0 represents saturated vapor pressure, solid and open symbols denote adsorption and desorption, respectively).

applications, we further characterized the sorption properties of **3b** at room temperature, a condition of practical interest.

CO_2, CH_4, and N_2 adsorption isotherms were measured for **3b** at 298 K (Figure 7), which show an obviously high affinity and capacity for CO_2. Detailed analysis shows that 1 L of **3b** can hold up to 52.9 L (1.7 mmol·g^{-1}) of CO_2 at 298 K and 1 atm. The three adsorption isotherms are fitted well by the Toth isotherm model (Figure 7).[39] Henry's Law selectivities of CO_2/CH_4 and CO_2/N_2 are calculated to be about 5.0 and 46, respectively. The CO_2/N_2 selectivity of **3b** is significantly higher than that of many other PCPs.[40]

The enthalpies of CO_2 adsorption (Q_{st}) were also calculated according to the Clausius−Clapeyron[41] equation from the adsorption isotherms measured at 283 and 298 K (Supporting Information, Figure S8). The corresponding adsorption enthalpy for CO_2 on **3b** is around 31−34 kJ·mol^{-1}, which are higher than the values for physisorption on purely silicious zeolite (ca. 27 kJ·mol^{-1})[42] and actived carbons (less than 26 kJ·mol^{-1}),[43,44] implying that there should be relatively strong interactions between the CO_2 molecules and the pore surfaces (e.g., the uncoordinated nitrogens).[45] Moreover, the Q_{st} does not monotonically decrease during uptake increase.[45] The sudden increase of adsorption enthalpy was rarely observed,[46] which may be attributed to the flexibility of the porous framework.[47]

To further characterize the size-selective adsorption of **3b**, benzene (C_6H_6) and cyclohexane (C_6H_{12}) adsorption studies were carried out. As revealed from the above sorption studies, the smallest slit should be expanded to allow the passage of CH_4, but larger molecules exceeding the upper limit of expansion should be obstructed. The difference in molecular sizes between C_6H_6 (3.3 × 6.6 × 7.3 Å^3) and C_6H_{12} (5.0 × 6.6 × 7.2 Å^3)[35] could be used to test the upper limit of framework flexibility.[36] Moreover, C_6H_6 and C_6H_{12} have a very small difference in their boiling points (C_6H_6, 80.1 °C; C_6H_{12}, 80.7 °C) and can form an azeotrope. It is a challenging problem in the petrochemical industry to separate them by distillation, as the latter is produced by hydrogenation of C_6H_6 in the C_6H_6/C_6H_{12} miscible system.[48]

The sorption isotherms of C_6H_6 and C_6H_{12} for **3b** were measured at 298 K (Figure 8). The profiles differ obviously between each other. In the case of C_6H_{12}, the adsorbed amount is only 16.7 mg·g^{-1} at P/P_0 = 0.88, which corresponds to 0.1 C_6H_{12} per Mn(dpt24)$_2$ unit, indicating particle surface adsorption. In contrast, the C_6H_6 adsorption indicates a type-I isotherm. The adsorbed amount for C_6H_6 is 201 mg·g^{-1} (1.3 C_6H_6 per Mn(dpt24)$_2$) at P/P_0 = 0.88, which is 12 times of that for C_6H_{12}. The discernible hysteresis observed for C_6H_6 may be attributed to the size effect and guest−host C−H···π or π···π interactions.[49] The C_6H_6-loaded powders still show the characteristic PXRD pattern of **3b**, indicating the framework stability after adsorption. The above findings imply that **3b** may be used for adsorptive-based separation of C_6H_6 and C_6H_{12}. Preliminary vapor adsorption study has also been carried out for toluene (molecular size: 8.3 × 6.6 × 4.0 Å^3)[35] (see Supporting Information, Figure S9), which revealed about 122 mg·g^{-1} saturation uptake, or about 0.66 toluene molecule per Mn(dpt24)$_2$ unit, indicating that the smallest slit of **3b** can expand to allow the passage of toluene molecules.

(38) Walton, K. S.; Snurr, R. Q. *J. Am. Chem. Soc.* **2007**, *129*, 8552.
(39) Malek, A.; Farooq, S. *AIChE J.* **1996**, *42*, 3191.
(40) Wang, B.; Cote, A. P.; Furukawa, H.; O'Keeffe, M.; Yaghi, O. M. *Nature* **2008**, *453*, 207.
(41) Shaw D. J. *Introduction to Colloid and Surface Chemistry*; Butterworth-Heinemann: Oxford, 1992.
(42) Dunne, J. A.; Rao, M.; Sircar, S.; Gorte, R. J.; Myers, A. L. *Langmuir* **1996**, *12*, 5896.
(43) Buss, E. *Gas Sep. Purif.* **1995**, *9*, 189.
(44) Himeno, S.; Komatsu, T.; Fujita, S. *J. Chem. Eng. Data* **2005**, *50*, 369.
(45) Caskey, S. R.; Wong-Foy, A. G.; Matzger, A. J. *J. Am. Chem. Soc.* **2008**, *130*, 10870.
(46) Bourrelly, S.; Llewellyn, P. L.; Serre, C.; Millange, F.; Loiseau, T.; Férey, G. *J. Am. Chem. Soc.* **2005**, *127*, 13519.
(47) Navarro, J. A. R.; Barea, E.; Rodriguez-Dieguez, A.; Salas, J. M.; Ania, C. O.; Parra, J. B.; Masciocchi, N.; Galli, S.; Sironi, A. *J. Am. Chem. Soc.* **2008**, *130*, 3978.
(48) Villaluenga, J. P. G.; Tabe-Mohammadi, A. *J. Membr. Sci.* **2000**, *169*, 159.
(49) Lin, X.; Blake, A. J.; Wilson, C.; Sun, X. Z.; Champness, N. R.; George, M. W.; Hubberstey, P.; Mokaya, R.; Schroder, M. *J. Am. Chem. Soc.* **2006**, *128*, 10745.

Conclusions

The self-assembly of a new MAF system based on Mn^{II} and an unsymmetrical 3,5-dipyridyl-1,2,4-triazolate have been studied for supramolecular isomerism and rational construction of PCPs. Two mononuclear complexes and three isomeric 2D PCPs have been synthesized. Remarkably, we have predicted the coordination modes, metal to ligand ratios, and stereo configurations of the octahedral metal centers, as well as the pore surface characters (uncoordinated nitrogen), which are important in supramolecular isomerism and rational construction of PCPs. Although ab initio prediction of a particular superstructure from the starting materials and synthetic condition is still impossible, some general principles are applicable for the observed structures and synthetic conditions.

Besides crystal engineering and supramolecular isomerism of the new MAF system, interesting chemical and physical properties were observed for the new compounds. The two mononuclear complexes exhibit reversible crystal-to-amorphous and crystal-to-crystal interconversions involving breakage and formation of coordination and hydrogen bonds, *trans-cis* conversion of stereo configuration, and rearrangement of molecules in the crystal lattices. Moreover, because of the *trans-cis* stereo configuration and different packing fashions, the isomeric, porous MAFs showed distinct porous structures, framework stabilities, and related sorption properties. Abnormal temperature-dependent sorption behavior for nitrogen, high selectivity and storage capacity for carbon dioxide, high benzene/cyclohexane adsorption ratio were connected to the structural characteristics including pore size, surface, and framework flexibility.

Acknowledgment. This work was supported by NSFC (Grant 20821001 & 20525102) and the "973 Project" (Grant 2007CB815302).

Supporting Information Available: Selected bond lengths and angles, additional structural plots, PXRD, TGA curves, additional sorption isotherms, as well as X-ray crystallographic files in CIF format. This material is available free of charge via the Internet at http://pubs.acs.org.